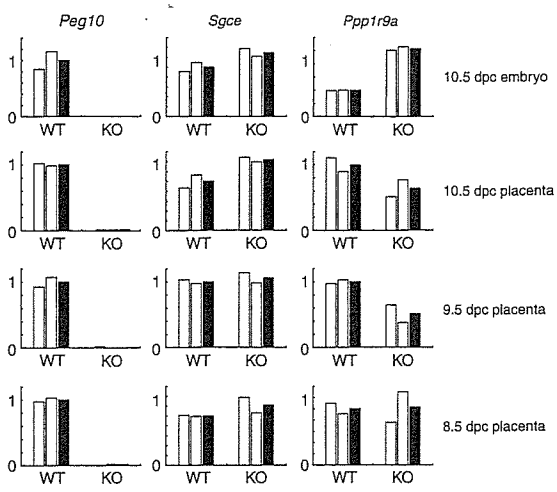

Figure 5 Relative expression levels of *Peg10*, *Sgce* and *Ppp1r9a* at different stages, as determined by quantitative RT-PCR The relative expression levels of 8.5- to 10.5-d.p.c. Pat-KO placentas and 10.5-d.p.c. Pat-KO embryos were determined by quantitative RT-PCR (as in **Fig. 4b**). Each reaction was performed at least three times. White bars represent single embryos and black bars represent the average of two embryos.

whereas genes that inhibit these growth have become maternally expressed during mammalian evolution[16]. Our results clearly show that *Peg10* conforms well to this hypothesis, as *Peg10* is paternally expressed and essential for the formation of the placenta, which functions to promote nutrient transfer from mother to fetus, as shown for the *Igf2* P0 transcript[17]. Therefore, we provide further evidence that the functional bias predicted by this hypothesis exists among imprinted genes.

Recently, RAG (the V(D)J recombinase)[18] and telomerase[19] have been shown or suggested to be derived from transposons and retrotransposons, respectively, indicating that some of these transposable elements have contributed to the acquisition of several new important genomic functions during evolution[20]. There are other reports that the rat IgE-binding protein contains a partial coding sequence of the retrotransposon intracisternal A particle (IAP)[21] and that the human *syncytin* gene[22], which functions in syncytiotrophoblast formation in placental tissues, is derived from a human endogenous retrovirus (HERV-W). Recently, mouse *syncytin-A* and *syncytin-B* genes have been isolated and, notably, have been found to be derived from similar but different retroviruses derived from the human HERV-W[23]. These findings also provide evidence that various species-specific retrotransposons play roles in different species. However, as far as we know, this is the first demonstration that an evolutionarily conserved mammal-specific, retrotransposon-derived gene has an essential function in development, at least in mice.

Recently, it has been reported that human PEG10 may have a carcinogenetic function in affecting cell cycle progression[24] or inhibiting apoptosis mediated by SIAH1 (ref. 25), and/or inhibiting TGF-β signaling by interacting with the TGF-β receptor ALK1 (ref. 26). Therefore, *PEG10* may have a wide variety of functions such as the regulation of cell growth and differentiation as well as placental function[1,8].

It is of great interest to learn the role of *Peg10* in the acquisition of the placenta during mammalian evolution, as it is highly conserved in eutherian mammals. Based on database searches, *Peg10* is not present in the *Fugu rubripes* (fish) or chicken genomes (**Supplementary Fig. 7**). Ancestral mammals might have developed this new organ, the placenta, from newly acquired, retrotransposon-derived genes, or endogenous genes present in oviparous animals might have been modified for placenta formation some time after the divergence of mammals and birds, more than 92 million years ago[27]. Further comparative genome analyses among eutherians marsupials, and monotremes may help to uncover the origin of *Peg10* in mammalian evolution. We found another ten homologues to the Sushi-ichi retrotransposon (called *Sirh* family genes) in the mouse and human genomes, including another paternally expressed gene, *Rtl1 (also* called *PEG11* in sheep)[3–6], which is located on the mouse distal chromosome 12, and *Ldoc1* (refs. 3,28) on the X chromosome. Similar conclusions have recently been reported by other researchers[29]. It will be fascinating to discover the functions of these evolutionarily conserved retrotransposon-derived genes, as well as those of *Peg10*.

METHODS

Deletion of the *Peg10* gene. We obtained 9.4-kb (nucleotides 6903–16254; AC084315) and 1.0-kb (nucleotides 20116-21135; AC084315) genomic fragments by screening the 129SvJ lambda genomic library (Stratagene). We used these fragments as the right- and left-arm sequences of a construct in which both *Peg10* ORFs were replaced with the neomycin resistance gene. After a 2-week incubation under G418 selection followed by electroporation of the linearized DNA into ES cells (CCE) of 129/SvEv mouse origin, we obtained 120 colonies. The genomic DNA of these colonies was checked by DNA blot analysis using DNA fragments of nucleotides 5300–6525 and nucleotides 21271–21766 as 5′-end and 3′-end probes, respectively.

The *Peg10*-targeted ES cells that resulted from homologous recombination of the construct were used to generate chimeric mice by blastocyst injection. From two male chimeras, germline transmission of the knockout allele was confirmed when pregnant female mice that had mated with a *Peg10* male chimera were dissected and their embryos analyzed.

PCR. Genomic DNA and total RNA samples were prepared from embryos and placentas at various stages using ISOGEN (Nippon Gene), as described previously[8]. The cDNA was synthesized from 1 μg of RNA using Superscript II reverse transcriptase (Life Technologies) with oligo-dT primer. For RT-PCR, 10 ng cDNA in a 100-μl reaction mixture containing 1× ExTaq buffer (TaKaRa), 2.5 mM dNTP mixture, primers and 2.5 units (U) ExTaq (TaKaRa) was subjected to 25–30 PCR cycles of 96 °C for 15 s, 65 °C for 30 s and 72 °C for 30 s in a Perkin Elmer GeneAmp PCR System 2400. Gene expression profiles were deduced from agarose gel electrophoresis of RT-PCR products with ethidium bromide staining. The primer sequences are available upon request.

Quantitative RT-PCR. The expression levels of 15 genes in the *Peg10* cluster and *Ascl2* were measured with the ABI PRISM 7700 using SYBR Green PCR Core Reagents (Applied Biosystems), which were designed to detect these cDNAs. The target cDNA fragments were cloned into plasmids to be used as standards in the quantitative analysis of gene expression. The relative expression ratios were normalized to the housekeeping gene β-*actin*. The primers for *DnciI* have been described previously[30]. The other primer sequences and conditions for their use are available upon request.

DNA methylation analyses of the *Peg10-Sgce* DMR. Genomic DNA samples were isolated from 9.5-d.p.c. embryos of JF1 × *Peg10*$^{+/-}$ F1 mice using ISOGEN, as described in the RT-PCR section. Purified genomic DNA was treated with a sodium bisulfite solution, and *Peg10-Sgce* DMR was amplified by PCR[8].

Generation of tetraploid aggregation chimeras. Electrofusion of two-cell–stage blastomeres collected from B6D2 F_1 females was used to produce wild-type tetraploid embryos. The fused embryos were cultured overnight in embryo culture medium in 5% CO_2 at 37 °C. Each eight-cell–stage diploid *Peg10* $^{+/-}$ embryo was aggregated overnight with a four-cell tetraploid embryo. Successfully aggregated embryo pairs at the morula or blastocyst stage were transferred to 2.5-d.p.c. pseudopregnant ICR recipients.

Histology. Pregnant mice that had mated with a *Peg10* knockout male were killed at 7.5, 8.5, 9.5, 10.5 and 11.5 d.p.c. Whole embryos were collected and immediately embedded in OCT. Sections from embedded embryos were cut in 7-μm sections. For hematoxylin and eosin staining or *in situ* hybridization, the sections were fixed in 4% paraformaldehyde before the standard staining procedures. The nuclei of the cell samples for *in situ* hybridization were stained with 2% methyl green.

Note: Supplementary information is available on the Nature Genetics website.

ACKNOWLEDGMENTS

We thank M.A. Surani and S. Barton for helpful suggestions on this manuscript. We also thank S. Aizawa for providing the DT-A vector, J. Miyazaki for the Cre-recombinase expression vector, E. Robertson for the CCE ES cells, H. Sasaki for the *Gallus gallus* genome, Y. Nakahara and M. Takabe of the Mitsubishi Kagaku Institute of Life Sciences for animal breeding, and S. Ichinose and T. Tajima of Tokyo Medical and Dental University and N. Kawabe and H. Hasegawa of Tokai University for assistance with the *in situ* hybridization experiments. This work was supported by grants from Research Fellowships of the Japan Society for the Promotion of Science for young Scientists (JSPS) to R.O.; the Asahi Glass Foundation to T.K.-I.; and CREST (the research program of the Japan Science and Technology Agency (JST)), the Uehara Memorial Science Foundation, the Ministry of Health, Labour and Welfare for Child Health and Development (14-C) and the Ministry of Education, Culture, Sports, Science and Technology of Japan to F.I.

COMPETING INTERESTS STATEMENT

The authors declare that they have no competing financial interests.

Published online at http://www.nature.com/naturegenetics
Reprints and permissions information is available online at http://npg.nature.com/reprintsandpermissions/

1. Ono, R. *et al.* A retrotransposon-derived gene, *PEG10*, is a novel imprinted gene located on human chromosome 7q21. *Genomics* **73**, 232–237 (2001).
2. Volff, J., Korting, C. & Schartl, M. Ty3/Gypsy retrotransposon fossils in mammalian genomes: did they evolve into new cellular functions? *Mol. Biol. Evol.* **18**, 266–270 (2001).
3. Butler, M., Goodwin, T., Simpson, M., Singh, M. & Poulter, R. Vertebrate LTR retrotransposons of the Tf1/sushi group. *J. Mol. Evol.* **52**, 260–274 (2001).
4. Charlier, C. *et al.* Human-ovine comparative sequencing of a 250-kb imprinted domain encompassing the callipyge (clpg) locus and identification of six imprinted transcripts: *DLK1, DAT, GTL2, PEG11*, anti*PEG11*, and *MEG8*. *Genome Res.* **11**, 850–862 (2001).
5. Lynch, C. & Tristem, M. A co-opted gypsy-type LTR-retrotransposon is conserved in the genomes of humans, sheep, mice, and rats. *Curr. Biol.* **13**, 1518–1523 (2003).
6. Seitz, H. *et al.* Imprinted microRNA genes transcribed antisense to a reciprocally imprinted retrotransposon-like gene. *Nat. Genet.* **34**, 261–262 (2003).
7. Shigemoto, K. *et al.* Identification and characterisation of a developmentally regulated mammalian gene that utilises -1 programmed ribosomal frameshifting. *Nucleic Acids Res.* **29**, 4079–4088 (2001).
8. Ono, R. *et al.* Identification of a large novel imprinted gene cluster on mouse proximal chromosome 6. *Genome Res.* **13**, 1696–1705 (2003).
9. Poulter, R. & Butler, M. A retrotransposon family from the pufferfish (fugu) Fugu rubripes. *Gene* **215**, 241–249 (1998).
10. Beechey, C., Cattanach, B.M., Blake, A. & Peters, J. *Mouse Imprinting Data and References*, http://www.mgu.har.mrc.ac.uk/research/imprinting (2003).
11. Nagy, A., Rossant, J., Nagy, R., Abramow-Newerly, W. & Roder, J.C. Derivation of completely cell culture-derived mice from early-passage embryonic stem cells. *Proc. Natl. Acad. Sci. USA* **90**, 8424–8428 (1993).
12. Guillemot, F. *et al.* Genomic imprinting of *Mash2*, a mouse gene required for trophoblast development. *Nat. Genet.* **9**, 235–242 (1995).
13. Surani, M.A., Barton, S.C. & Norris, M.L. Development of reconstituted mouse eggs suggests imprinting of the genome during gametogenesis. *Nature* **308**, 548–550 (1984).
14. McGrath, J. & Solter, D. Completion of mouse embryogenesis requires both the maternal and paternal genomes. *Cell* **37**, 179–183 (1984).
15. Sturm, K.S., Flannery, M.L. & Pedersen, R.A. Abnormal development of embryonic and extraembryonic cell lineages in parthenogenetic mouse embryos. *Dev. Dyn.* **201**, 11–28 (1994).
16. Moore, T. & Haig, D. Genomic imprinting in mammalian development: a parental tug-of-war. *Trends Genet.* **7**, 45–49 (1991).
17. Constancia, M. *et al.* Placental-specific IGF-II is a major modulator of placental and fetal growth. *Nature* **417**, 945–948 (2002).
18. Agrawal, A., Eastman, Q.M. & Schatz, D.G. Transposition mediated by *RAG1* and *RAG2* and its implications for the evolution of the immune system. *Nature* **394**, 744–751 (1998).
19. Nakamura, T.M. & Cech, T.R. Reversing time: origin of telomerase. *Cell* **92**, 587–590 (1998).
20. Smit, A.F. Interspersed repeats and other mementos of transposable elements in mammalian genomes. *Curr. Opin. Genet. Dev.* **9**, 657–663 (1999).
21. Toh, H., Ono, M. & Miyata, T. Retroviral gag and DNA endonuclease coding sequences in IgE-binding factor gene. *Nature* **318**, 388–389 (1985).
22. Mi, S. *et al.* Syncytin is a captive retroviral envelope protein involved in human placental morphogenesis. *Nature* **403**, 785–789 (2000).
23. Dupressoir, A. *et al.* Syncytin-A and syncytin-B, two fusogenic placenta-specific murine envelope genes of retroviral origin conserved in Muridae. *Proc. Natl. Acad. Sci. USA* **102**, 725–730 (2005).
24. Tsou, A.P. *et al.* Overexpression of a novel imprinted gene, *PEG10*, in human hepatocellular carcinoma and in regenerating mouse livers. *J. Biomed. Sci.* **10**, 625–635 (2003).
25. Okabe, H. *et al.* Involvement of PEG10 in human hepatocellular carcinogenesis through interaction with SIAH1. *Cancer Res.* **63**, 3043–3048 (2003).
26. Lux, A. *et al.* Human retroviral gag- and gag-pol-like proteins interact with the TGF-β receptor ALK1. *J. Biol. Chem.* **280**, 8482–8493 (2005).
27. Hedges, S.B. The origin and evolution of model organisms. *Nat. Rev. Genet.* **3**, 838–849 (2002).
28. Nagasaki, K. *et al.* Identification of a novel gene, *LDOC1*, down-regulated in cancer cell lines. *Cancer Lett.* **140**, 227–234 (1999).
29. Brandt, J. *et al.* Transposable elements as a source of genetic innovation: expression and evolution of a family of retrotransposon-derived neogenes in mammals. *Gene* **345**, 101–111 (2005).
30. Horike, S., Cai, S., Miyano, M., Cheng, J.F. & Kohwi-Shigematsu, T. Loss of silent-chromatin looping and impaired imprinting of *DLX5* in Rett syndrome. *Nat. Genet.* **37**, 31–40 (2005).

RADIATION RESEARCH 166, 877–882 (2006)
0033-7587/06 $15.00

Trp53 Affects the Developmental Anomaly of Clefts of the Palate in Irradiated Mouse Embryos but not Clefts of the Lip with or without the Palate

Shota Narai,[a,b] Yasumitsu Kodama,[b] Yoshitaka Maeda,[c] Minesuke Yokoyama,[c] Ritsuo Takagi[b] and Ryo Kominami[a,d,1]

Departments of [a] Molecular Genetics and [b] Oral Health Science, Niigata University Graduate School of Medical and Dental Sciences, [c] Center for Bioresource-Based Researches, Brain Research Institute; and [d] Center for Transdisciplinary Research, Niigata University, Asahimachi 1-757, Niigata 951-8510, Japan

Narai, S., Kodama, Y., Maeda, Y., Yokoyama, M., Takagi, R. and Kominami, R. Trp53 Affects the Developmental Anomaly of Clefts of the Palate in Irradiated Mouse Embryos but not Clefts of the Lip with or without the Palate. *Radiat. Res.* 166, 877–882 (2006).

***Trp53*-deficient mice exhibit increased incidences of developmental anomalies when irradiated, probably due to lack of Trp53-dependent apoptosis. A/J strain-derived CL/Fr mice develop clefts of the lip with or without the palate (CL/P) in approximately one-fifth of the embryos. We produced *Trp53*-deficient CL/Fr mice and examined the susceptibility to spontaneous development of CL/P and clefts of palate only (CPO), which differ in their developmental mechanisms, CL/P resulting from clefts of the primary palate and CPO from clefts of the secondary palate. The effect of radiation on the two phenotypes was also studied. Unexpectedly, no increase in the frequency of CL/P was observed under either condition, indicating that *Trp53* deficiency does not contribute to genesis of CL/P. On the other hand, radiation enhanced the incidence of CPO in *Trp53*$^{+/+}$ embryos but not in *Trp53*$^{+/-}$ and *Trp53*$^{-/-}$ embryos, suggesting that the absence or presence of only one allele of *Trp53* is insufficient to hinder differentiation and proliferation of cells involved in the secondary palate formation. These results indicate that Trp53 function adversely affects the development of CPO when certain damaging agents such as radiation are given.** © 2006 by Radiation Research Society

INTRODUCTION

Craniofacial anomalies comprise a significant component of morbid birth defects. They require surgical, dental, medical and behavioral interventions and impose a substantial economic burden (*1*). Clefts of the lip and palate affect about one in 700 births; half of the cases are nonsyndromic without other anomalies (*2, 3*). There are some particular geographic areas having high incidences; this suggests genetic founder effects or the existence of environmental triggers (*3*). Genetic studies in humans implicate transforming growth factor alpha (*TGFA*), *MSX1, BMP4, FGF10* and *IRF6* in clefts of the lip with or without the palate (CL/P) (*1, 3, 4*). On the other hand, many mouse models have been described that exhibit clefts of the lip or palate as part of the phenotype. The CL/Fr and A/J mouse strains are classic models for human nonsyndromic clefting because they develop clefts without other abnormalities. CL/Fr mice, generated by crossing Morgan's stock MSL mice with A/J mice, spontaneously develop CL/P at a frequency of approximately one in five of embryos, whereas A/J mice develop CL/P at a frequency of approximately one in ten embryos (*5–7*). Due to the high susceptibility to CL/P, these mice have been used for the CL/P studies (*3, 7*). Morphogenetic analyses suggest that clefts of the primary palate resulting in CL/P are different in mechanism from clefts of the secondary palate that involve the palate only (CPO) (*1–3*).

Although genetic variations play a substantial role for craniofacial anomalies, the role that the environment plays in modulating genetic effects is equally important. Ionizing radiation is an environmental component that causes DNA damage and apoptosis, which are thought to initiate teratogenicity. Experimental studies with mice have established that irradiation in the organogenesis period induces high incidences of prenatal death and developmental abnormalities, including clefts of the lip and palate (*8, 9*). Radiation, like numerous drugs and environmental chemicals that cause anomalies, interacts with and is modified by radiation-responsible genes. The *Trp53* tumor suppressor gene is one such gene and plays a key role in eliminating cells with DNA damage in developing tissues by assisting DNA repair and apoptosis (*10, 11*). Interestingly, *Trp53*-deficient mice exhibit spontaneous developmental anomalies such as mid-brain exencephaly (*12, 13*) and also show higher teratogenicity than *Trp53* wild-type mice when they are irradiated (*14, 15*). This enhancement is ascribed to loss of Trp53-dependent apoptosis. Therefore, susceptibility to

[1] Address for correspondence: Departments of Molecular Genetics and Center for Transdisciplinary Research, Niigata University, Asahimachi 1-757, Niigata 951-8510, Japan; e-mail: rykomina@med.niigata-u.ac.jp.

clefts in the CL/Fr strain may increase when Trp53 deficiency is introduced. Furthermore, it is possible that exposure to radiation may raise the frequency of CL/P and/or CPO in Trp53-deficient CL/Fr mice. Thus we produced the *Trp53*$^{-/-}$ CL/Fr mice and investigated whether loss of Trp53 influences frequencies of CL/P and CPO in embryos with and without irradiation.

MATERIALS AND METHODS

Mice and Mating

The CL/Fr mice used in this study were provided from the Second Department of Oral Maxillofacial Surgery, Aichi Gakuin University (Nagoya, Japan) in 1988. The mice were mated with *Trp53*$^{+/-}$ mice of BALB/c background and the F_1 mice carrying a Trp53-deficient allele were backcrossed with CL/Fr mice to produce *Trp53*$^{+/-}$ CL/Fr mice. The marker-assisted protocol (*16*) was employed for this, and the *Trp53*$^{+/-}$ CL/Fr mice generated after six-time backcrossing were used for the present study. Sixty MIT markers distributed throughout the mouse genome were used for the marker-assisted protocol as follows: D1Mit432, D1Mit530, D1Mit46, D1Mit12, D1Mit17, D2Mit5, D2Mit295, D2Mit92, D2Mit199, D3Mit1, D3Mit29, D3Mit200, D4Mit149, D4Mit174, D4Mit43, D4Mit338, D4Mit344, D5Mit112, D5Mit24, D6Mit312, D6Mit9, D6Mit339, D7Mit130, D7Mit362, D8Mit18, D8Mit9, D8Mit318, D9Mit22, D9Mit347, D10Mit246, D10Mit194, D10Mit230, D10Mit151, D11Mit106, D11Mit26, D11Mit222, D11Mit12, D12Mit88, D12Mit122, D12Mit8, D13Mit266, D13Mit287, D14Mit2, D14Mit234, D14Mit200, D15Mit11, D15Mit17, D15Mit272, D16Mit32, D16Mit4, D16Mit203, D17Mit246, D17Mit176, D17Mit76, D18Mit19, D18Mit122, D19Mit32, D19Mit41, D19Mit90, D19Mit71. The PCR program consisted of one cycle of 10 min at 95°C, 40 cycles of 30 s at 95°C, 30 s at 55°C, and 1 min at 72°C, and one cycle of 10 min at 72°C. After six backcrossings, the *Trp53*$^{+/-}$ CL/Fr mice were mated to each other and used for experiments. In addition to natural mating, we used embryos that were prepared using the *in vitro* fertilization method. Fertilized eggs at the two-cell stage, which had been prepared with eggs and sperm obtained from *Trp53*$^{+/-}$ CL/Fr mice, were transplanted into pseudopregnant ICR females. Mice used in this study were maintained under specific-pathogen-free conditions in the animal colony of Niigata University. All experimental procedures involving the mice were approved by the ethics committee for animal experimentation of Niigata University.

Irradiation

Two female mice were mated with one male overnight and were checked for copulation plugs the following morning. The gestational age of the embryos was calculated using 0:00 a.m. on the day of plug detection as day 0 and hour 0. Pregnant females at 9.5 days of gestation were given a whole-body dose of 2 Gy radiation from a broad-beam ^{137}Cs source. The dose was delivered at 1 Gy per minute. At irradiation, each unanesthetized mouse was placed in the ventilated circular holder to minimize its movement during exposure so the whole body would receive the radiation dose uniformly. The holder allowed the mouse to sit in a normal position but did not allow the animal to turn around.

Examination of CL/P and CPO

At 18.5 days of gestation (E18.5), embryos were removed from the placental membranes and weighed. Under a dissecting microscope, embryos or uterine contents were classified into normal, resorption or death, cleft of lip and palate, and other malformations. CL/P or CPO was determined by scoring the lip and palate by after removal of the lower jaw. Cleft of the primary palate with or without the secondary palate was classified as CL/P, and cleft of the secondary palate only was classified as CPO (*6, 17*).

Genotyping

Embryos and uterine contents were genotyped for *Trp53* with PCR using a set of three primers: the forward primer of *Trp53* in the intron 4, 5′-GACCTCCGTTCTCTCTCCT-C-3′, the reverse of *Trp53* in the intron 6, 5′-GACGCACAAACCAAAACAAAATTAC-3′, and the forward of *neo* derived from the *neo* cassette, 5′-TTCTATCGCCTTCTTGACGAGT-3′. The PCR program consists of one cycle of 10 min at 94°C, 40 cycles of 30 s at 94°C, 30 s 60°C and 30 s at 72°C, followed by one cycle of 10 min at 72°C (*18*).

Western Blotting

Pregnant females on 9.5 days of gestation were exposed to 2 Gy (1 Gy/min) of γ rays. Embryos were removed 4, 8, 12 and 16 h after irradiation, homogenized and suspended in a buffer containing 40 m*M* Tris-HCl (pH 7.5), 0.25 *M* sucrose, 25 m*M* KCl and 5 m*M* $MgCl_2$. After the homogenate was mixed with an equal volume of the lysis buffer containing 0.125 *M* Tris-HCl (pH 6.8), 10% sucrose, 10% SDS, 10% 2-ME and 0.004% bromophenol blue, an aliquot (200 μg) was electrophoresed in 14% SDS-PAGE gel and blotted onto Hybond membranes (Amersham Pharmacia Biotech, Piscataway, NJ) (*19*). Antibodies used here were as follows: anti-Trp53 (no. sc-1312), anti-actin (no. sc-1615), and HRP-anti-goat IgG (no. sc-2020) purchased from Santa Cruz Biotechnology, and HRP-anti-rabbit IgG (no. NA934V) purchased from Amersham Pharmacia Biotech. Protein bands were visualized using a chemiluminescence detection kit (ECL plus, Amersham Pharmacia Biotechnology).

Statistics

χ^2 test was used for statistical analysis with StatView-J 5.0 software on a Macintosh personal computer. Differences were considered to be statistically significant when the *P* value was less than 0.05.

RESULTS

CL/Fr mice maintained in our animal facility developed CL/P and CPO at frequencies of 19% and 0.3%, respectively, when 293 fetuses were examined at embryonic day 18.5 (E18.5). The frequencies were similar to those reported previously (*5–7*). However, other anomalies such as excencephaly were not observed in our inspections. A *Trp53*-deficient allele was introduced into CL/Fr mice by backcrossing *Trp53*$^{+/-}$ BALB/c mice with CL/Fr mice. Table 1 shows the incidences of deaths including resorptions, body weights and incidences of clefts in CL/Fr embryos of the three different *Trp53* genotypes. *Trp53*$^{+/+}$ CL/Fr embryos exhibited CL/P at a frequency of 16%, similar to 19% for the parental CL/Fr mice. This excluded the possibility that BALB/c-derived chromosomal regions remaining in the *Trp53*$^{+/+}$ CL/Fr mice affect the CL/P incidence.

The frequency of embryonic deaths in completed placentas was low, 11.1% in *Trp53*$^{+/+}$ and 9.8% in *Trp53*$^{+/-}$ CL/Fr embryos and only 3.1% in *Trp53*$^{-/-}$ CL/Fr embryos. Average body weight did not differ among them. On the other hand, CL/P was observed in 20 (18%) of a total of 109 embryos examined. The frequency in *Trp53*$^{-/-}$ embryos was 13%, similar to the frequencies of 16% in *Trp53*$^{+/+}$ embryos and 24% in *Trp53*$^{+/-}$ embryos. No CPO was observed. This result indicated no marked influence of *Trp53* genotype on CL/P or CPO, which was an unexpected

TABLE 1
Effects of *Trp53* Genotypes on Frequency of Death, Cleft and other Anomalies

Trp53 genotype	Placentas examined	Deaths[a]	Lives	Body weight (g)	Cleft		Other anomalies
					CLP	CPO	
+/+	36	4 (11.1%)	32	0.98	5 (15.6%)	0	0
+/−	51	5 (9.8%)	46	1.00	11 (23.9%[b])	0	0
−/−	32	1 (3.1%)	31	0.98	4 (12.9%[c])	0	0

[a] Deaths including resorptions.
[b] $P = 0.34$ in comparison with +/+.
[c] $P = 0.77$ in comparison with +/+.

finding, since *Trp53*$^{-/-}$ mice were expected to be susceptible to clefts, as described in the Introduction.

It is well known that radiation induces embryonic deaths and teratogenicity (*8, 9*). Hence we examined the effect of radiation on those phenotypes, including the incidences of CL/P and CPO in the mice (Table 2). As shown in Fig. 1A, exposure of *Trp53*$^{+/+}$ CL/Fr embryos at the organogenesis period (E9.5) to 2 Gy radiation induced deaths at an incidence of 39% (49/125) in completed placentas, whereas irradiated CL/Fr embryos of *Trp53*$^{+/-}$ and *Trp53*$^{-/-}$ genotypes showed only 8% (8/95) and 12% (4/33) incidences of deaths, respectively. This high incidence of deaths in *Trp53*$^{+/+}$ CL/Fr embryos is consistent with previous reports (*14, 15*). However, we found much lower incidences in *Trp53*$^{+/-}$ and *Trp53*$^{-/-}$ CL/Fr embryos, and the difference between *Trp53*$^{+/+}$ and *Trp53*$^{+/-}$ CL/Fr embryos (*P* value less than 0.001) revealed haploinsufficiency of Trp53 for Trp53-dependent induction of embryonic deaths. Figure 1B shows another difference in the body weight. *Trp53*$^{+/+}$ CL/Fr embryos weighed approximately 0.75 g on the average, much less than the 0.91 g and 0.97 g of CL/Fr embryos of *Trp53*$^{+/-}$ and *Trp53*$^{-/-}$ genotypes, respectively (*P* values in both cases less than 0.001). This may be parallel to the difference in the frequency of embryonic deaths. Those differences in embryonic deaths and body-weight loss may be accounted for by induction of cell cycle arrest and apoptosis in irradiated cells by Trp53.

We examined the expression of Trp53 at various times after irradiation of CL/Fr mouse embryos with 2 Gy at E9.5 (Fig. 2). Accumulation of Trp53 protein reached its maximum 4 h after radiation exposure in both *Trp53*$^{+/+}$ and *Trp53*$^{+/-}$ embryos, whereas no expression was detected in *Trp53*$^{-/-}$ embryos. However, the level of Trp53 expression differed between them, with expression being approximately half as much in *Trp53*$^{+/-}$ embryos. The results confirmed the dependence of Trp53 expression on the dose of the allele in CL/Fr embryos that were exposed to γ rays at the same dose used for the induction of clefts of the lip and the palate.

Irradiated embryos of different *Trp53* genotypes exhibited little difference in the CL/P phenotype (Table 2, Fig. 1C). The incidence of CL/P in *Trp53*$^{+/+}$ and of *Trp53*$^{+/-}$ CL/Fr embryos was 11% (8/76) and 6% (5/87), respectively, whereas that in *Trp53*$^{-/-}$ embryos was 24% (7/29), higher than the other two incidences. However, this incidence of 24% did not differ much from the 18% that was observed in unirradiated embryos. In contrast, an enhancement of CPO incidence was observed in irradiated *Trp53*$^{+/+}$ embryos (Table 2, Fig. 1D). The frequency was as high as 29% (22/76), significantly higher than the values of 1% (1/87) in *Trp53*$^{+/-}$ embryos (*P* value less than 0,001) and 3% (1/29) in *Trp53*$^{-/-}$ embryos ($P = 0.005$). The low incidence in *Trp53*$^{+/-}$ embryos may also be due to *Trp53* haploinsufficiency. These results suggest that the presence of both *Trp53* wild-type alleles, but not a single allele, in embryos increases the incidence of CPO after irradiation, probably by inducing an excess of apoptosis or possibly cell cycle arrest that impairs normal development. This result was also unexpected, because *Trp53*$^{-/-}$ mice are thought to be susceptible to radiation-induced malformation, including CPO. On the other hand, gross phenotypic anomalies were not found after irradiation except for tail

TABLE 2
Effects of *Trp53* Genotype on Frequency of Death, Cleft and other Anomalies in Embryos Irradiated on Day 9.5 of Gestation

Trp53 genotype	Placentas examined	Deaths[a]	Lives	Body weight (g)	Cleft		Other anomalies
					CLP	CPO	
+/+	125	49 (39.2%)	76	0.75	8 (10.5%)	22 (28.9%)	18[b] (23.7%)
+/−	95	8 (8.4%)	87	0.91	5 (5.7%)	1 (1.1%)	30[c] (34.5%)
−/−	33	4 (12.1%)	29	0.97	7 (24.1%)	1 (3.4%)	0

Note. *P* values of deaths, average body weight, and clefts (CLP and CPO) are shown in Fig. 1.
[a] Deaths including resorptions.
[b] Fifteen tail anomalies and three umbilical hernias.
[c] All tail anomalies.

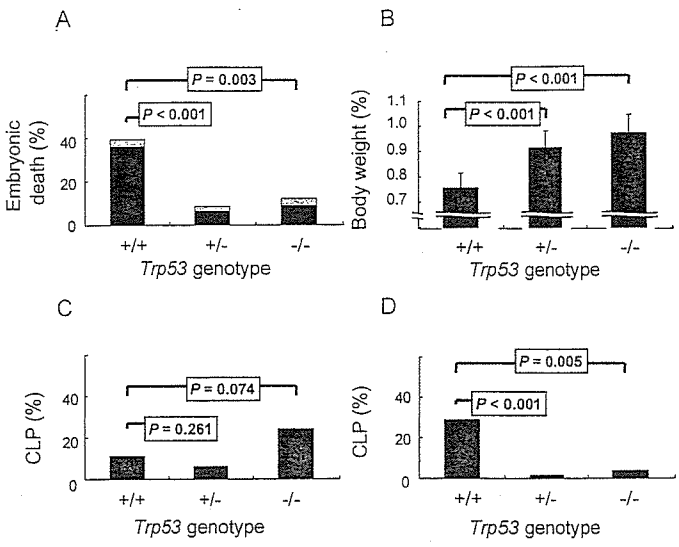

FIG. 1. Analyses of mouse embryos of $Trp53^{+/+}$, $Trp53^{+/-}$ and $Trp53^{-/-}$ genotypes at embryonic day 18.5 that were irradiated with 2 Gy at embryonic day 9.5. Panel A: Incidence of deaths, most of which are resorptions (black). Panel B: Average body weight of living embryos. Panel C: Incidence of CLP. Panel D: Incidence of CPO. Error bars represent standard deviations.

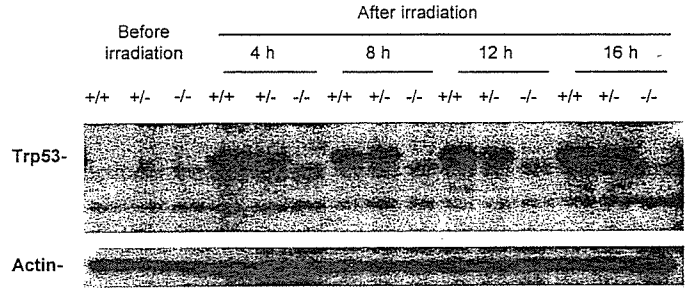

FIG. 2. Expression of Trp53 protein in mouse embryos of $Trp53^{+/+}$, $Trp53^{+/-}$ and $Trp53^{-/-}$ genotypes after irradiation. Pregnant females on 9.5 day of gestation were exposed to 2 Gy (1 Gy/min) of γ rays. Embryos were removed 4, 8, 12 and 16 h after irradiation and subjected to Western blotting.

anomalies. The frequency of tail anomalies was 24% and 35% in $Trp53^{+/+}$ and $Trp53^{+/-}$ CL/Fr embryos, respectively, whereas no case was found in $Trp53^{-/-}$ embryos (Table 2). This case of tail anomalies did not exhibit an influence of *Trp53* haploinsufficiency.

DISCUSSION

This study examined the susceptibility of Trp53-deficient CL/Fr mice to CL/P and CPO with and without radiation exposure. In the *Trp53* wild-type CL/Fr strain, approximately one-fifth of the embryos spontaneously developed CL/P; however, no influence of Trp53 deficiency on CL/P frequency was observed in either irradiated or unirradiated embryos. In contrast, radiation exposure enhanced the CPO incidence in $Trp53^{+/+}$ embryos, consistent with previous reports (*8, 9*), but no enhancement was observed in $Trp53^{+/-}$ and $Trp53^{-/-}$ embryos. This result was not our initial prediction because lack of Trp53-dependent apoptosis has been reported to increase teratogenicity (*14, 15*). This may be ascribed to differences in the phenotypes and mouse strains examined.

The developmental processes leading to the formation of the upper lip and palate have been studied at the morphogenetic and molecular levels; this helps us understand the etiology of CL/P and CPO (*4, 20, 21*). A cleft lip is thought to result from a failure of fusion between the maxillary and medial nasal processes or between the opposing medial and lateral nasal processes during embryogenesis (*21, 22*). The failure of proper lip formation secondarily affects palatal contact, resulting in some cases in cleft palate. Therefore, CL is often accompanied by CP. On the other hand, fusion between the primary and secondary palates occurs much later in embryogenesis than lip formation. Fusion for palate formation occurs between the secondary palatal shelves, which arise bilaterally from the maxillary processes.

Histological sections of the developmental upper lip of the human and mouse show the formation of an epithelial seam between the intermaxillary segment and maxillary processes that is subsequently replaced by connective tissues (*23*). Similar pictures are seen in fusion of the secondary palate (*23, 24*). The medial edge epithelia (MEE), consisting of basal columnar cells covered by flat peridermal cells, promote the formation of a seam. The peridermal cells undergo region-restricted apoptosis in chick embryos and also in mouse and rat embryos, resulting in their sloughing off (*24, 25*). This apoptosis has been proposed to function for breakdown of the seam for the replacement by connective tissues, thereby playing an important role in fusion of the lip and palate (*24, 25*). Trp53-dependent apoptosis occurs when cells undergo various cellular stresses (*10, 11*). Apoptosis of this type is probably different from the apoptosis observed in the epithelial seam cells during lip formation, because the introduction of *Trp53* deficiency into CL/Fr mice did not increase the incidence of cleft lip. Likewise, since $Trp53^{-/-}$ CL/Fr mice did not show an elevated incidence of CPO in embryos when they were irradiated, Trp53-dependent apoptosis is also distinct from the apoptosis seen in the MEE cells during palate development.

Epithelial filopodia in highly localized primary fusion areas anchor into the surface of the opposing prominences by penetrating between surface cells and are reinforced by the accumulation of large cellular extensions and adherence junctions (*23, 26*). Interestingly, such filopodial attachments are much more reduced in A/WySn and CL/Fr mouse embryos than in those of the C57BL/6 strain, which has a negligible spontaneous incidence of CL/P (*7, 27*). This suggests some defect in developing cells and tissues in those mouse embryos. Obviously, proliferation and differentiation are important morphogenetic mechanisms because cells in different parts of the embryo divide at different rates and differentiate properly to generate new structures.

Accordingly, another mechanism is proposed for lip and palate formation. This is transformation of the midline epithelial seam to the mesenchyme, which may play an important role in the replacement of the MEE by connective tissues (*23, 26*). Our finding that Trp53-dependent apoptosis is a cause of CPO in irradiated embryos may be accounted for by inhibition of growth of developing tissues by that apoptosis. Therefore, though it is not known which cells in the developing tissues undergo apoptosis, such apoptosis might hinder the proliferation of MEE cells to impair the formation of the secondary palate. Alternatively, the proliferation of other cells such as MEE-supporting cells may be inhibited in irradiated *Trp53*$^{+/+}$ embryos, and this inhibition may cause CPO. Marked loss of body weight was observed in those embryos, indicating robust cell cycle arrest and/or massive apoptosis in many different developing tissues.

Trp53$^{-/-}$ and *Trp53*$^{+/-}$ CL/Fr embryos both showed significantly lower incidences of radiation-induced deaths and CPO than *Trp53*$^{+/+}$ embryos, and those embryos also weighed more. This indicates that the presence of a single copy of *Trp53* is not sufficient to hinder proliferation and possible differentiation of cells involved in the development of palate when embryos are irradiated during the organogenesis period. Dependence of Trp53 expression on the copy number of *Trp53* was confirmed in the CL/Fr embryos (see Fig. 2). The haploinsufficiency may be due to Trp53-dependent induction of cell cycle arrest and apoptosis. This is consistent with previous data on teratogenicity in irradiated *Trp53*$^{+/+}$ mouse embryos (*28*). On the other hand, *Trp53* haploinsufficiency for tumor suppression has been demonstrated in a variety of tumors by retention of a single wild-type allele in some of the tumors that developed (*29, 30*). Loss of one allele is thought to confer an effect, though weak, on the selective advantage in tumor development.

In conclusion, our results indicate that Trp53-dependent apoptosis does not affect CL/P incidence, although apoptosis is considered to be important for embryonic development. On the other hand, Trp53-dependent apoptosis plays a key role in the development of CPO when mouse embryos are exposed to radiation during the organogenesis period. This confirms that administration of DNA-damaging agents is a certain risk factor for CPO in mice and probably in humans.

ACKNOWLEDGMENT

This work was supported by a grant-in-aid from by the Ministry of Education, Culture, Sports, Science and Technology of Japan.

Received: March 28, 2006; accepted: June 23, 2006

REFERENCES

1. P. Stanier and G. E. Moore, Genetics of cleft lip and palate: Syndromic genes contribute to the incidence of non-syndromic clefts. *Hum. Mol. Genet.* **13** (Review Issue 1), R73–R81 (2004).
2. A. P. Vanderas, Incidence of cleft lip, cleft palate, and cleft lip and palate among races: A review. *Cleft Palate J.* **24**, 216–225 (1987).
3. J. C. Murray, Gene/environment causes of cleft lip and/or palate. *Clin. Genet.* **61**, 248–256 (2002).
4. J. C. Murray and B. C. Schutte, Cleft palate: Players, pathways, and pursuits. *J. Clin. Invest.* **113**, 1676–1678 (2004).
5. S. Bornstein, D. G. Trasler and F. C. Fraser, Effect of the uterine environment on the frequency of spontaneous cleft lip in CL/FR mice. *Teratology* **3**, 295–298 (1970).
6. D. M. Juriloff and F. C. Fraser, Genetic maternal effects on cleft lip frequency in A/J and CL/Fr mice. *Teratology* **21**, 167–175 (1980).
7. G. Millicovsky, L. J. Ambrose and M. C. Johnston, Developmental alterations associated with spontaneous cleft lip and palate in CL/Fr mice. *Am. J. Anat.* **164**, 29–44 (1982).
8. L. B. Russell and W. L. Russell, An analysis of the changing radiation response of the developing mouse embryo. *J. Cell Physiol.* **43**, 103–149 (1954).
9. G. Callas and B. E. Walker, Palate morphogenesis in mouse embryos after x-irradiation. *Anat. Rec.* **145**, 61–71 (1963).
10. A. J. Giaccia and M. B. Kastan, The complexity of p53 modulation: Emerging patterns from divergent signals. *Genes Dev.* **12**, 2973–2983 (1998).
11. P. Fei and W. S. El-Deiry, P53 and radiation responses. *Oncogene* **22**, 5774–5783 (2003).
12. V. P. Sah, L. D. Attardi, G. J. Mulligan, B. O. Williams, R. T. Bronson and T. Jacks, A subset of p53-deficient embryos exhibit exencephaly. *Nat. Genet.* **10**, 175–180 (1995).
13. J. F. Armstrong, M. H. Kaufman, D. J. Harrison and A. R. Clarke, High-frequency developmental abnormalities in p53-deficient mice. *Curr. Biol.* **5**, 931–936 (1995).
14. T. Norimura, S. Nomoto, M. Katsuki, Y. Gondo and S. Kondo, p53-dependent apoptosis suppresses radiation-induced teratogenesis. *Nat. Med.* **2**, 577–580 (1996).
15. S. Nomoto, A. Ootsuyama, Y. Shioyama, M. Katsuki, S. Kondo and T. Norimura, The high susceptibility of heterozygous p53$^{+/-}$ mice to malformation after foetal irradiation is related to sub-competent apoptosis. *Int. J. Radiat. Biol.* **74**, 419–429 (1998).
16. P. Markel, P. Shu, C. Ebeling, G. A. Carlson, D. L. Nagle, J. S. Smutko and K. J. Moore, Theoretical and empirical issues for marker-assisted breeding of congenic mouse strains. *Nat. Genet.* **17**, 280–284 (1997).
17. M. Nagata, N. Amin, Y. Kannari, M. Hayatsu, Y. Ohashi and A. Oguro, Isolated maxillary bending in CL/FR strain mice: Observation of craniofacial deformity and inheritance pattern. *Cleft Palate Craniofac. J.* **34**, 101–105 (1997).
18. T. Kubota, Y. Yoshikai, Y. Tamura, Y. Mishima, Y. Aoyagi, O. Niwa and R. Kominami, Comparison of properties of spontaneous and radiation-induced mouse thymic lymphomas: Role of Trp53 and radiation. *Radiat. Res.* **163**, 159–164 (2005).
19. Y. Wakabayashi, H. Watanabe, J. Inoue, N. Takeda, J. Sakata, Y. Mishima, J. Hitomi, T. Yamamoto, M. Utsuyama and R. Kominami, Bcl11b is required for differentiation and survival of αβ T lymphocytes. *Nat. Immunol.* **4**, 533–539 (2003).
20. C. Martínez-Álvarez, C. Tudela, J. Pérez-Miguelsanz, S. O'Kane, J. Puerta and M. W. Ferguson, Medial edge epithelial cell fate during palatal fusion. *Dev. Biol.* **220**, 343–357 (2000).
21. R. Jiang, J. O. Bush and A. C. Lidral, Development of the upper lip: Morphogenetic and molecular mechanisms. *Dev. Dyn.* **235**, 1125–1166 (2005).
22. S. G. Gong and C. Guo, Bmp4 gene is expressed at the putative site of fusion in the midfacial region. *Differentiation* **71**, 228–236 (2003).
23. E. D. Hay, The mesenchymal cell, its role in the embryo, and the remarkable signaling mechanisms that create it. *Dev. Dyn.* **233**, 706–720 (2005).
24. F. Vaziri Sani, K. Hallberg, B. D. Harfe, A. P. McMahon, A. Linde and A. Gritli-Linde, Fate-mapping of the epithelial seam during palatal fusion rules out epithelial–mesenchymal transformation. *Dev. Biol.* **285**, 490–495 (2005).

25. R. Cuervo and L. Covarrubias, Death is the major fate of medial edge epithelial cells and the cause of basal lamina degradation during palatogenesis. *Development* **131**, 15–24 (2004).

26. A. Nawshad and E. D. Hay, TGFβ3 signaling activates transcription of the LEF1 gene to induce epithelial mesenchymal transformation during mouse palate development. *J. Cell Biol.* **163**, 1291–1301 (2003).

27. D. G. Trasler and L. Ohannessian, Ultrastructure of initial nasal process cell fusion in spontaneous and 6-aminonicotinamide-induced mouse embryo cleft lip. *Teratology* **28**, 91–101 (1983).

28. B. Wang, H. Ohyama, K. Haginoya, T. Odaka, T. Yamada and I. Hayata, Prenatal radiation-induced limb defects mediated by Trp53-dependent apoptosis in mice. *Radiat. Res.* **154**, 673–679 (2000).

29. S. Venkatachalam, Y. P. Shi, S. N. Jones, H. Vogel, A. Bradley, D. Pinkel and L. A. Donehower, Retention of wild-type p53 in tumors from p53 heterozygous mice: Reduction of p53 dosage can promote cancer formation. *EMBO J.* **17**, 4657–4667 (1998).

30. W. D. Cook and B. J. McCaw, Accommodating haploinsufficient tumor suppressor genes in Knudson's model. *Oncogene* **19**, 3434–3438 (2000).

Journal of Reproduction and Development, Vol. 52, No. 4, 2006

—Full Paper—

The Relationship between Sperm Morphology and *In Vitro* Fertilization Ability in Mice

Yasuhiro KAWAI[1,2], Tomoko HATA[1], Osamu SUZUKI[1,2] and Junichiro MATSUDA[1,2]

[1]Department of Veterinary Science, National Institute of Infectious Diseases and [2]Laboratory of Experimental Animal Models, National Institute of Biomedical Innovation, Osaka, Japan

Abstract. *In vitro* fertilization (IVF) is widely used in reproduction research, but the sperm of some inbred strains of mice yield low fertilization rates in IVF. To determine the cause of this problem, we examined the effect of epididymal sperm morphology, in particular, tail bending and the presence and type of cytoplasmic droplet (CD), on fertilizability *in vitro*. Sperm suspensions were obtained from the following five strains: C57BL/6J, BALB/cA, C3H/HeN, DBA/2J, and 129 × 1/SvJ. The sperm were fixed in 10% formalin and three parts of the sperm, namely the head, tail, and CD, were examined. We recorded the proportion of abnormal sperm heads and hairpins at the neck; tails were categorized as straight, proximal bent, or distal bent; and the CDs were categorized as none, light-type, and heavy-type. Based on these parameters, we determined the correlations between sperm morphology and fertilizability *in vitro*, as judged by IVF using ICR oocytes. The proportion of sperm with a hairpin neck was higher in strain C57BL/6J, while abnormal head morphology occurred significantly more often in strain BALB/cA. The percentage of sperm with a proximal bent tail was highest in strain DBA/2J and lowest in strain 129 × 1/SvJ. A heavy-type CD was observed more frequently in the 129 × 1/SvJ and C57BL/6J strains than in the other three strains in which a light-type CD predominated. The rank order of the fertilization rates was 129 × 1/SvJ < C57BL/6J < C3H/HeN < BALB/cA < DBA/2J. In addition, fertilization rate was positively correlated with a proximal bent tail, but negatively correlated with a heavy-type CD and distal bent tail. This new classification system establishes that the morphological characteristics of epididymal sperm differ among inbred strains of mice and that tail and CD morphology are closely related to fertilization ability in IVF. Thus, our results provide a novel method for assessing the quality of mouse sperm used for IVF.

Key words: Cytoplasmic droplet, Epididymal sperm, *In vitro* fertilizability, Sperm morphology

(J. Reprod. Dev. 52: 561–568, 2006)

Inbred strains of laboratory mice are the most frequently used animals in basic research, including reproduction and genetic research. Strain C57BL/6 is used in studies on cardiovascular biology, developmental biology, diabetes and obesity, genetics, immunology, neurobiology, and sensorineural research. The BALB/c strain is used to produce monoclonal antibodies. The 129 × 1/Sv strain produces targeted mutations owing to the availability of several embryonic stem cell lines. DBA/2 mice are valuable in cardiovascular biology, neurobiology, and sensorineural research, while strain C3H/HeJ is used as a general-purpose animal model for cancer, immunology, inflammation, sensorineural, and cardiovascular research. Recent advances in reproductive techniques have allowed the production of various transgenic and knockout animals that serve as useful models of human diseases and allow

Accepted for publication: May 9, 2006
Published online: June 7, 2006
Correspondence: Y. Kawai (e-mail: kaya@nibio.go.jp)

analyses of new gene functions.

In vitro fertilization (IVF) is a widely used technique in reproduction research, fertility treatment, and cryopreservation of animal embryos; however, the spermatozoa of some inbred strains of mice yield low fertilization rates in IVF. In rodents, epididymal sperm are required for IVF because the sperm do not become functional for fertilization in the process termed epididymal maturation until they arrive at the cauda epididymis [1–3]. Sperm morphology has been shown to influence fertilizability *in vitro*, and the low rate of successful IVF in the BALB/c strain [4–7] is thought to be due to the high proportion of sperm with a morphologically abnormal head [8]. Obtaining fertilized embryos with IVF is also difficult with the 129/SvJ strain, which is commonly used to establish embryonic stem cell lines [7]. In human infertility studies, the structure of the sperm tail, in addition to abnormalities in the structure of the head, has been shown to influence the fertilization rate. Moreover, the cytoplasmic droplet (CD), which is derived from the cytoplasm in the sperm cell and is believed to drop off from the sperm tail during sperm maturation [9], is also related to infertility in humans and some domestic animals [10, 11]. Recently, Burruel *et al.* [12], Yanagimachi [13], and Yanagimachi *et al.* [14] reported that intracytoplasmic sperm injection (ICSI), a powerful reproductive technique, overcomes the problem of low fertilization rates. In this approach, oocytes are directly injected with abnormal-headed sperm, immotile sperm, or round spermatids, but this technique is complex and requires a well-trained technician. Therefore, the development of a more useful IVF technique for the maintenance and preservation of various inbred mice strains is essential.

To determine the cause of the low fertility rate, we examined the effect of epididymal sperm morphology, particularly the tail and CD, on the fertilization ability of sperm from five inbred mice strains, C57BL/6J, BALB/cA, C3H/HeN, DBA/2J, and 129 × 1/SvJ. First, we classified the morphological features of three parts of the sperm, the head, tail, and CD. Second, we examined the fertilization rates of epididymal sperm from these strains by IVF of ovulated oocytes of Slc:ICR female mice. Finally, we evaluated the impact of sperm morphology, classified according to our new criteria, on the fertilization rates by searching for correlations between the morphological characteristics of the epididymal sperm and the fertilization rates in IVF.

Materials and Methods

Mice

Sperm were obtained from the cauda epididymides of male mice from five inbred strains. Strains C57BL/6J Jms and 129 × 1/SvJ Jms were purchased from Japan SLC (Hamamatsu, Japan), and strains BALB/cA Jcl, C3H/HeN Jcl, and DBA/2J Jcl were purchased from CLEA Japan (Tokyo, Japan). Female Slc:ICR mice older than 8 weeks of age were purchased from Japan SLC. Animal experiments were carried out according to the guidelines for animal experiments of the National Institute of Infectious Diseases, Tokyo, Japan.

Culture media

Human tubal fluid medium (HTF), as described by Quinn [15], was used for IVF. HTF consists of 101.6 mM NaCl, 4.96 mM KCl, 0.20 mM $MgSO_4 \cdot 7H_2O$, 0.37 mM KH_2PO_4, 2.04 mM $CaCl_2 \cdot 2H_2O$, 25 mM $NaHCO_3$, 2.73 mM glucose, 0.33 mM Na pyruvate, 21.40 mM Na DL-lactate (60%), 0.075 mg penicillin/ml, 0.050 mg streptomycin/ml, and 4% BSA (fraction V). We used M16 medium for *in vitro* culture of embryos [16].

Preparation of sperm suspensions

The epididymides were removed from mature 12- to 14-week-old mice that had been euthanized by cervical dislocation [17]. First, the epididymis was cut in the cauda region using iridectomy scissors. A drop containing a dense mass of spermatozoa was then picked up quickly with the tips of tweezers and put into 0.4 ml of HTF that had been kept in a CO_2 incubator (5% CO_2 in air, 37 C).

Classification of sperm morphology and motility for five inbred strains of mice

Sperm were collected from the sperm suspensions after a 5-min incubation in a CO_2 incubator. To examine sperm morphology, the suspended sperm were fixed with 10% formalin, placed on a glass slide, and observed under phase-contrast microscopy. The different forms of abnormal sperm heads, including triangular, collapsed, and hammer head (Figs. 1a, b), and the

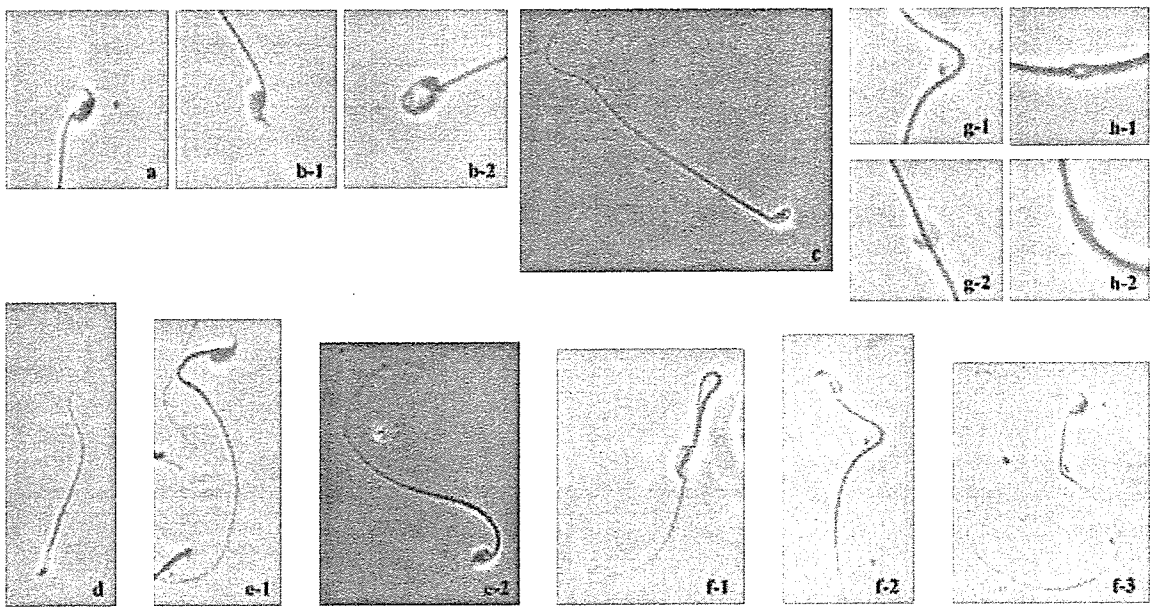

Fig. 1. Morphological classification of mouse epididymal sperm. Phase-contrast micrographs of fixed spermatozoa. (a, b) Differences in sperm-head morphology: normal (a) and abnormal (b-1, 2) forms. (c) Sperm with a hairpin neck. (d–f) Differences in the sperm tail: straight type (d), proximal bent tail (e-1, 2), and distal bent tail (f-1–3). (g, h) Differences in the cytoplasmic droplet (CD): heavy-type CD (g-1, 2) and light-type CD (h-1, 2).

presence of a hairpin at the neck (Fig. 1c) were also noted. Sperm tail morphology was classified into three categories as follows (Figs. 1d–f): straight tail, proximal bent tail (*i.e.*, the tail curved in the midpiece), and distal bent tail (*i.e.*, the tail was angled at the end of the midpiece), which included the angled and hairpin forms. CDs were assigned to one of three categories as follows: none, heavy-type, and light-type CDs (Figs. 1g, h). From the suspended sperm of the five males from each strain, 200 spermatozoa/male were counted and screened.

In vitro fertilization

The suspended sperm were preincubated for 1 h under 5% CO_2 in air at 37 C before being used for insemination. After preincubation, the sperm suspension was introduced into a 0.4-ml droplet of HTF in a plastic dish to produce a concentration of 2.4–4.6 × 10^6 spermatozoa/ml in each suspended sperm drop. Immature female mice were injected intraperitoneally with 5 IU pregnant mare serum gonadotrophin (PMSG; Teikokuzouki, Tokyo, Japan), and 48–49 h later, they were injected with 5 IU human chorionic gonadotrophin (hCG; Sankyou, Tokyo, Japan). The superovulated mice were euthanized 14.5–15.5 h after hCG injection. The oviduct was isolated, placed in a dish containing the preincubated diluted sperm suspension, and covered with silicon oil (Sigma-Aldrich, St. Louis, MO, USA). The cumulus-oocyte complexes were dissected out of the oviduct and introduced into the sperm suspension drop. Six hours after insemination, the cumulus cells were stripped by pipetting with 0.1% hyaluronidase (Sigma-Aldrich) in HTF.

Evaluating sperm penetration and two-cell formation

Half of the denuded oocytes were mounted, fixed, dehydrated, stained with 0.25% lacmoid, and examined under a phase-contrast microscope, as described by Toyoda and Chang [17]. An oocyte was judged as penetrated when it had an enlarged sperm head and/or pronucleus and a corresponding sperm tail in the vitellus. Oocytes with spermatozoa in the perivitelline space were not considered to be penetrated. Fertilization rates were calculated from the number of penetrated oocytes. Denuded oocytes in the remaining half were washed three times with 0.1 ml of M16, transferred into 0.1 ml of M16, and cultured in an atmosphere of 5% CO_2 in air at 37 C. At 24 h after

Table 1. Morphology of sperm in five inbred mouse strains

	% of sperm without a CD	% of sperm with a cytoplasmic droplet (CD)		Sperm tail morphology %			Hairpin[d] %	Abnormal sperm head %
		Light	Heavy	Straight	Proximal bent	Distal bent		
129xl/SvJ	28.7 ± 2.2[a]	40.6 ± 4.0[a]	31.7 ± 4.2[a]	32.2 ± 1.3[ac]	4.5 ± 0.9[a]	62.5 ± 4.5[a]	7.5 ± 0.8[b]	3.3 ± 0.4[a]
C57BL/6J	44.9 ± 4.6[b]	32.4 ± 4.3[b]	33.9 ± 2.8[ab]	42.8 ± 2.8[b]	5.6 ± 0.8[a]	51.3 ± 2.7[b]	10.4 ± 0.7[a]	5.6 ± 0.2[a]
C3H/HeN	35.2 ± 2.4	44.3 ± 2.7[a]	19.5 ± 0.9[bc]	41.8 ± 2.5[a]	19.6 ± 1.0[b]	37.1 ± 2.5[b]	6.5 ± 0.5[b]	10.7 ± 0.3[b]
BALB/cA	48.6 ± 3.3[b]	41.9 ± 2.9[a]	9.5 ± 1.3[c]	53.5 ± 3.6[b]	25.4 ± 2.7[b]	20.9 ± 2.1[c]	6.6 ± 2.3[b]	21.2 ± 1.8[c]
DBA/2J	34.6 ± 3.9	57.9 ± 3.3[c]	7.5 ± 1.5[c]	35.2 ± 2.2[c]	40.9 ± 3.4[c]	23.8 ± 3.4[c]	3.1 ± 1.1[b]	4.1 ± 1.4[a]

Values are means ± SEM (n=5).

[a, b, c]: Values with different superscripts are significantly different within each column ($p<0.05$).

[d]: Hairpin at the neck.

insemination, the rate of two-cell formation was determined under an inverted phase-contrast microscope.

Evaluating sperm morphology in the perivitelline space

IVF for evaluation of sperm morphology in the perivitelline space was performed, as described above. The sperm suspension obtained from DBA/2J Jcl was introduced into a HTF droplet to produce a concentration of 1.0×10^6 spermatozoa/ml. Oocytes were obtained from Slc:ICR mice. One-hour after insemination, oocytes were fixed and observed under a phase-contrast microscope.

Statistical analysis

The values for the proportions of total oocytes that showed penetration, pronuclear formation, and two-cell formation were subjected to arcsine transformation in each replicate. The transformed values were analyzed using one-way ANOVA. For significant differences detected by ANOVA, one-to-one comparisons were carried out using Tukey's multiple range test. The values for sperm morphological parameters were analyzed using the same methods. The correlational trends between the fertilization rate and each morphological parameter were calculated using Fisher's *rz* transformation.

Results

Morphological features of the sperm of each inbred strain

The morphology of the epididymal sperm from the five inbred strains of mice (129 × 1/SvJ, C57BL/6J, BALB/cA, C3H/HeN, and DBA/2J) were characterized and then compared. The results are summarized in Table 1. The percentage of sperm with a light-type CD was significantly higher in strain DBA/2J than in the other strains, and the percentage of sperm with a heavy-type CD was significantly lower in strain DBA/2J than in strains 129 × 1/SvJ and C57BL/6J. With respect to tail morphology, the percentage of sperm with proximal bent tails was significantly higher in strains C3H/HeN, BALB/cA, and DBA/2J than in strains 129 × 1/SvJ and C57BL/6J. Compared with the other strains, the C57BL/6J strain had a significantly higher percentage of sperm with a hairpin neck. The percentage of abnormal heads was significantly higher in strain BALB/cA than in the other strains.

Fertilization ability of spermatozoa and two-cell formation of the five inbred strains

Oocytes derived from Slc:ICR female mice were inseminated *in vitro* with the epididymal sperm of the five inbred strains. First, the morphology and weight of the testes and epididymides of each strain was examined, and no significant differences were found (data not shown). Penetration, pronuclear formation, and two-cell formation rates were significantly higher in strain DBA/2J than in the other four strains (Table 2). Penetration and pronuclear formation rates were significantly higher in strain BALB/cA than in strains 129 × 1/SvJ, C57BL/6J, and C3H/HeN. Moreover, the differences in the pronuclear formation rate were greater among individuals in strains C57BL/6J, BALB/cA, and C3H/HeN than among individuals in strains DBA/2J and BALB/cA.

Table 2. Fertilization and developmental rates with sperm from five inbred mouse strains

	No. of trails	No. of females	No. of oocytes ovulated	No. of abnormal oocytes	No. of oocytes checked	% of oocytes penetrated	Pronuclear formation %	No. of embryos cultured	2-cell formation %
129xl/SvJ	5	13	232	32	109	31.3[a] (4.9)	23.7[a] (3.4)	91	54.0[ab] (11.2)
C57BL/6J	5	15	261	21	119	29.5[a] (3.2)	29.5[a] (9.1)	121	42.4[a] (6.3)
C3H/HeN	5	13	253	12	120	47.8[a] (3.3)	40.1[a] (7.4)	121	53.8[a] (6.7)
BALBA/cA	10	27	441	49	193	68.9[b] (3.8)	64.6[b] (10.0)	199	71.2[b] (5.7)
DBA/2J	5	13	199	27	84	97.7[c] (4.3)	97.7[c] (1.3)	88	98.9[c] (1.0)

Values are means ± (SEM).
[a, b, c]: Values with different superscripts are significantly different within each column ($P<0.05$).

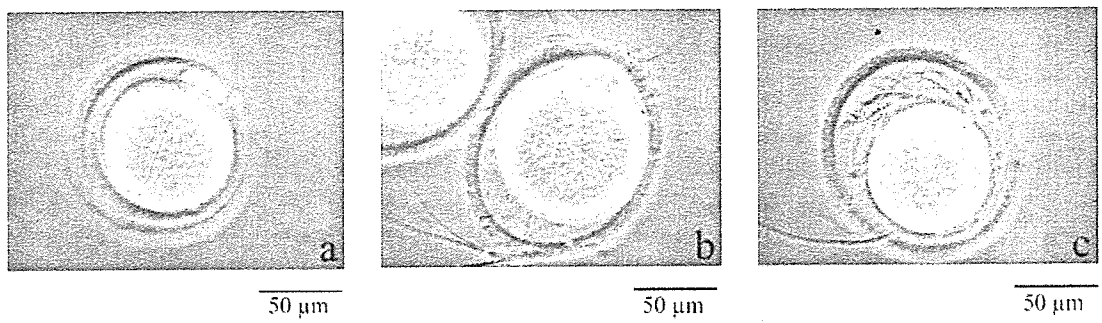

Fig.2. Morphology of sperm in the perivitelline space. (a, b) Monospermic oocytes. Sperm with straight (a) and proximal bent (b) tails penetrated in the perivitelline space. (c) Polyspermic oocytes. Note that one sperm in the perivitelline space had a light-type CD (white circle).

Evaluating sperm morphology in the perivitelline space

Sperm were observed in the perivitelline space of oocytes 1 h after insemination. The penetration and polyspermic rates were 45.8 and 17.2%, respectively. Sperm in the monospermic oocytes had straight or proximal bent tails without a CD (Figs. 2a, b), whereas sperm in polyspermic oocytes had a light-type CD (Fig. 2c). No sperm with a distal bent tail and/or heavy CD were observed in the perivitelline space.

Correlation between the fertilization rate and morphological parameters of epididymal spermatozoa in mice

Correlations between the fertilization rate and morphological parameters of the epididymal sperm were determined using Fisher's *rz* transformation (Table 3). The fertilization rate was highly correlated with a proximal bent tail and inversely correlated with a heavy-type CD and distal bent tail. In addition, the proportion of sperm with a proximal bent tail was positively correlated with the proportion of sperm with a light-type CD and negatively correlated with the proportion of sperm with a heavy-type CD. The opposite was true for the proportion with a distal bent tail. The proportion of sperm with a light-type CD was highly correlated with the proportion of sperm with a hairpin neck.

Discussion

The new classification of epididymal sperm morphology described in this study focuses on the

Table 3. Correlation coefficients among morphological parameters of sperm in five inbred mouse strains

	Fertilization rate	Without a CD[a]	Light CD[a]	Heavy CD[a]	Straight tail	Proximal bent tail	Distal bent tail	Hairpin[b]	Abnormal head
Fertilization rate	1.000	0.107	0.655	−0.812*	−0.046	0.818*	−0.696*	−0.572	0.351
Without a CD[a]	0.107	1.000	−0.500	−0.339	0.593	0.000	0.391	0.505	0.468
Light CD[a]	0.655	−0.500	1.000	−0.636	−0.446	0.728*	−0.345	−0.852*	−0.054
Heavy CD[a]	−0.812	−0.339	−0.636	1.000	−0.057	−0.788*	0.737*	0.474	−0.380
Straight tail	−0.046	0.593	−0.446	−0.057	1.000	−0.217	−0.489	0.376	0.490
Proximal bent tail	0.818	0.000	0.728	−0.788	−0.217	1.000	−0.742*	−0.592	0.070
Distal bent tail	−0.696	0.391	−0.345	0.737	−0.489	−0.742	1.000	0.277	−0.409
Hairpin[b]	−0.572	0.505	−0.852	0.474	0.376	−0.592	0.277	1.000	−0.083
Abnormal head	0.351	0.468	−0.054	−0.380	0.490	0.070	−0.409	−0.083	1.000

[a]: Cytoplasmic droplet. [b]: Hairpin at the neck. *: Values with superscripts are significantly correlated ($p<0.05$).

CD and sperm tail and on their relationship to fertilizability. Accordingly, the morphological characteristics of the epididymal sperm were found to differ among the inbred strains of mice, with the morphology of the tail and CD being closely related to fertilization ability in IVF. A high percentage of heavy-type CD in the epididymal sperm correlated with a low fertilization rate in IVF, although there was no significant difference in the morphology or weight of the testis and epididymis among the strains. These findings suggest that the fertilization rate of CD-containing sperm is strain-specific and that the CD shedding system and function of the CD may differ among strains. The CD of epididymal sperm is derived from the cytoplasm in the sperm cell and is believed to drop from the sperm tail during descent through the epididymis [9]. In mice, most sperm in the proximal epididymis have a CD, and this has been suggested to play a role in volume regulation [18]. The shape of the CD is related to infertility in some human patients [10] and is thus thought to affect fertilizability *in vivo* and *in vitro*. Although the shedding system and function of the CD are still unclear, the protein 15-LOX [19] and molecules recognized by anti-ubiquitin antibody [20] have been reported to be involved in CD function and removal. Further analyses are needed to determine whether the distribution of these molecules is strain-dependent, as is the presence of a CD.

The present study also revealed that the bending pattern of sperm tails is closely linked to the form of the CD. A proximal bent tail correlated positively with the presence of a light-type CD and negatively with the presence of a heavy-type CD, whereas the opposite was true for a distal bent tail. Correlations between the shape of the sperm tail and the presence of a CD are not well documented. However, flagellar angulation in the sperm of *c-ros* knockout mice was found at the site of the CD [21], and the shapes of the tail and CD were independently related to the fertilization rate [10]. In fact, sperm with straight or proximal bent type tails without a CD were observed in the perivitelline space 1 h after insemination. This result indicated that morphologically normal sperm participated in fertilization. In addition, although we did not observe a light-type CD in the perivitelline space of monospermic oocytes, we thought that sperm with a light-type CD might be able to fertilize an oocyte. Although it is yet to be determined whether these morphological parameters affect fertilization ability, including motility and capacitation, in IVF, either directly or indirectly, our results show that these morphological parameters may be useful for evaluating the fertilizability of sperm in IVF.

The proportion of sperm with abnormal head morphology was found to have less of an effect on the fertilization rate in IVF than the shape of the sperm tail and the presence of a CD. The proportion of sperm with abnormal heads was higher in the BALB/cA strain than in the other strains, but was lower than that previously reported [4, 13]. Difficulties in using BALB/cA sperm to fertilize oocytes *in vitro* are therefore probably due to the high rate of abnormal heads. Abnormal sperm heads have been reported in mutant mice and some gene knockout mice, and the sperm from these mice showed low fertilization rates in IVF [22–25]. However, ICSI can be used to overcome this problem and produce embryos [26].

We did not determine whether BALB/cA sperm with abnormal heads were specifically able to fertilize oocytes, but the BALB/cA strain most likely had a high fertilization rate because the majority of the sperm had a normal head. Moreover, the effects associated with abnormalities of the sperm tail and CD were more serious than those related to morphological abnormalities of the sperm head.

The rate of two-cell formation in our IVF study was strain-dependent. In addition, except for a higher rate in the BALB/cA strain, the rates in our study were similar to those in previous reports [5, 7]. However, our IVF results cannot be directly compared to those of previous reports because the oocytes in this study were derived from ICR females only. Preliminary experiments using BALB/cA oocytes and BALB/cA sperm under the same conditions as in the present study showed a higher fertilization rate than those described in earlier reports (data not shown). Interestingly, fertilization rates determined by sperm penetration rates differed from those based on two-cell formation rates in strains 129 × 1/SvJ and C57BL/6J, implying that the percentage of parthenogenetically activated embryos was higher in these two strains than in the other three strains. In addition, 4-cell formation rates in strains 129 × 1/SvJ and C57BL/6J were 27.9% and 28.6%, respectively (data not shown). These findings support the results of Sonnenberg *et al.* [27], who showed that paternal genetic background influences the developmental ability of early embryos. Similarly, in the present study, paternal genetic background also appeared to affect the rate of two-cell formation and parthenogenesis of the embryos. However, detailed investigations are needed to determine whether a direct relationship exists between these phenomena and epididymal sperm morphology.

Our new system of epididymal sperm classification will be useful in evaluation of sperm morphology in inbred mice. In addition, certain morphological characteristics of epididymal sperm, in particular, a heavy-type CD, distal bent tail, and hairpin neck, were shown to be closely related to low fertilizability *in vitro*, suggesting that these morphologies had an influence. Investigation of the factors underlying these morphological features will no doubt lead to improved IVF techniques and provide insight into the mechanisms of spermatozoa maturation. In the meantime, our classification system offers a new method of assessing sperm quality in IVF.

Acknowledgments

This work was supported by a grant from the Ministry of Health, Labour and Welfare, Japan.

References

1. **Tulsiani DR, Orgebin-Crist MC, Skudlarek MD.** Role of luminal fluid glycosyltransferases and glycosidases in the modification of rat sperm plasma membrane glycoproteins during epididymal maturation. *J Reprod Fertil Suppl* 1998; 53: 85–97.
2. **Topfer-Petersen E.** Carbohydrate-based interactions on the route of a spermatozoon to fertilization. *Hum Reprod Update* 1999; 5: 314–329.
3. **Suarez SS.** The oviductal sperm reservoir in mammals: mechanisms of formation. *Biol Reprod* 1998; 58(5): 1105–1107.
4. **Kishikawa H, Tateno H, Yanagimachi R.** Chromosome analysis of BALB/c mouse spermatozoa with normal and abnormal head morphology. *Biol Reprod* 1999; 61: 809–812.
5. **Szczygiel MA, Kusakabe H, Yanagimachi R, Whittingham DG.** Separation of motile populations of spermatozoa prior to freezing is beneficial for subsequent fertilization *in vitro*: a study with various mouse strains. *Biol Reprod* 2002; 67: 287–292.
6. **Nakagata N.** Cryopreservation of mouse spermatozoa. *Mamm Genome* 2000; 11: 572–576.
7. **Sztein JM, Farley JS, Mobraaten LE.** *In vitro* fertilization with cryopreserved inbred mouse sperm. *Biol Reprod* 2000; 63: 1774–1780.
8. **Wu HT, Chou CK, Lin CS, Huang MC.** Effects of glucose concentration on *in vitro* fertilization in BALB/c mice. *Reprod Domest Anim* 2003; 38: 470–474.
9. **Yanagimachi R.** Mammalian fertilization. In: Knobil E, Neill JD (eds.), The Physiology of Reproduction, 2nd ed. New York: Raven Press; 1994: 189–317.
10. **Cooper TG.** Cytoplasmic droplet: the good, the bad or just confusing? *Hum Reprod* 2005; 20: 9–11.
11. **Cooper TG, Yeung CH, Fetic S, Sobhani A, Nieschlag E.** Cytoplasmic droplets are normal structures of human sperm but are not well preserved by routine procedures for assessing

sperm morphology. *Hum Reprod* 2004; 19: 2283–2288.
12. **Burruel VR, Yanagimachi R, Whitten WK.** Normal mice develop from oocytes injected with spermatozoa with grossly misshapen heads. *Biol Reprod* 1996; 55: 709–714.
13. **Yanagimachi R.** Intracytoplasmic sperm injection experiments using the mouse as a model. *Hum Reprod* 1998; 13 (Suppl 1): 87–98.
14. **Yanagimachi R, Wakayama T, Kishikawa H, Fimia GM, Monaco L, Sassone-Corsi P.** Production of fertile offspring from genetically infertile male mice. *Proc Natl Acad Sci USA* 2004; 101: 1691–1695.
15. **Quinn P, Kerin JF, Warnes GM.** Improved pregnancy rate in human *in vitro* fertilization with the use of a medium based on the composition of human tubal fluid. *Fertil Steril* 1985; 44: 493–498.
16. **Whittingham DG.** Culture of mouse ova. *J Reprod Fertil* 1971; 13: 7–12.
17. **Toyoda Y, Chang MC.** Fertilization of rat eggs *in vitro* by epididymal spermatozoa and the development of eggs following transfer. *J Reprod Fertil* 1974; 36: 9–22.
18. **Yeung CH, Anapolski M, Sipila P, Wagenfeld A, Poutanen M, Huhtaniemi I, Nieschlag E, Cooper TG.** Sperm volume regulation: maturational changes in fertile and infertile transgenic mice and association with kinematics and tail angulation. *Biol Reprod* 2002; 67: 269–275.
19. **Fischer KA, Van Leyen K, Lovercamp KW, Manandhar G, Sutovsky M, Feng D, Safranski T, Sutovsky P.** 15-Lipoxygenase is a component of the mammalian sperm cytoplasmic droplet. *Reproduction* 2005; 130: 213–222.
20. **Kuster CE, Hess RA, Althouse GC.** Immunofluorescence reveals ubiquitination of retained distal cytoplasmic droplets on ejaculated porcine spermatozoa. *J Androl* 2004; 25: 340–347.
21. **Yeung CH, Sonnenberg-Riethmacher E, Cooper TG.** Infertile spermatozoa of c-ros tyrosine kinase receptor knockout mice show flagellar angulation and maturational defects in cell volume regulatory mechanisms. *Biol Reprod* 1999; 61: 1062–1069.
22. **Akutsu H, Tres LL, Tateno H, Yanagimachi R, Kierszenbaum AL.** Offspring from normal mouse oocytes injected with sperm heads from the azh/azh mouse display more severe sperm tail abnormalities than the original mutant. *Biol Reprod* 2001; 64: 249–256.
23. **Mendoza-Lujambio I, Burfeind P, Dixkens C, Meinhardt A, Hoyer-Fender S, Engel W, Neesen J.** The *Hook1* gene is non-functional in the abnormal spermatozoon head shape (azh) mutant mouse. *Hum Mol Genet* 2002; 11: 1647–1658.
24. **Nakamura T, Yao R, Ogawa T, Suzuki T, Ito C, Tsunekawa N, Inoue K, Ajima R, Miyasaka T, Yoshida Y, Ogura A, Toshimori K, Noce T, Yamamoto T, Noda T.** Oligo-astheno-teratozoospermia in mice lacking Cnot7, a regulator of retinoid X receptor beta. *Nat Genet* 2004; 36: 528–533.
25. **Nishizono H, Shioda M, Takeo T, Irie T, Nakagata N.** Decrease of fertilizing ability of mouse spermatozoa after freezing and thawing is related to cellular injury. *Biol Reprod* 2004; 71: 973–978.
26. **Du ZF, Wales RG.** Some effects of genotype and composition of the culture medium on the development of mouse zygotes *in vitro*. *Reprod Fertil Dev* 1993; 5: 405–415.
27. **Sonnenberg-Riethmacher E, Walter B, Riethmacher D, Godecke S, Birchmeier C.** The c-ros tyrosine kinase receptor controls regionalization and differentiation of epithelial cells in the epididymis. *Genes Dev* 1996; 10: 1184–1193.

ELSEVIER

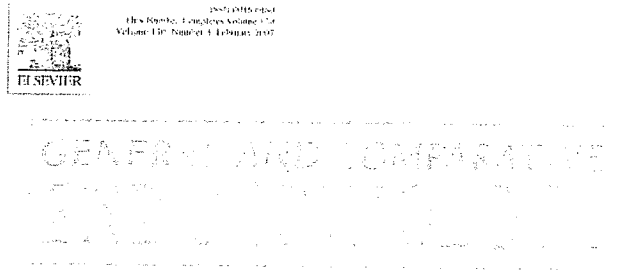

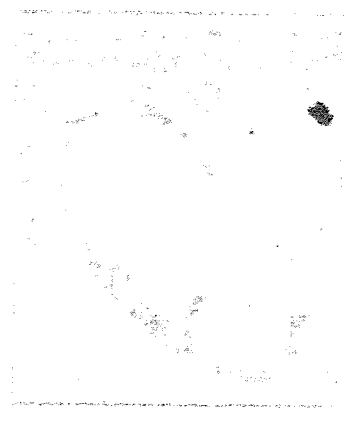

Published with the Division of Comparative Endocrinology of The Society for Integrative and Comparative Biology, the European Society for Comparative Endocrinology, the Asia and Oceania Society for Comparative Endocrinology, and the Japan Society for Comparative Endocrinology

www.elsevier.com/locate/ygcen

Available online at
ScienceDirect
www.sciencedirect.com

Available online at www.sciencedirect.com
ScienceDirect
General and Comparative Endocrinology 150 (2007) 514–519
GENERAL AND COMPARATIVE ENDOCRINOLOGY
www.elsevier.com/locate/ygcen

Communications in Genomics and Proteomics

Analyses of the cDNA and genomic DNA sequences encoding the luteinizing hormone β-subunit precursor protein in the rabbit

Osamu Suzuki *, Minako Koura, Yoko Noguchi, Kaoru Takano, Kozue Uchio-Yamada, Junichiro Matsuda

Laboratory of Experimental Animal Models, National Institute of Biomedical Innovation, Saito-Asagi 7-6-8, Ibaraki, Osaka 567-0085, Japan

Received 5 June 2006; revised 20 September 2006; accepted 30 September 2006
Available online 13 November 2006

Abstract

To examine the molecular basis for efficient induction of superovulation in the rabbit, we determined the cDNA sequences of the luteinizing hormone β-subunit (LHB) from Japanese White (JW), New Zealand White (NZW), and Dutch-Belted (Dutch) rabbits, and we compared these LHB sequences with those of other mammals. Using 5′- and 3′-rapid amplification of cDNA ends (RACE) with pituitary cDNA libraries, we found that the LHB cDNAs of all three breeds are the same length (523 bp from the 5′-end to the polyA site) and have putative AATAAA polyadenylation signal sequences at nucleotides 504 to 509. Northern blot analysis indicated that the ~600-nt mRNA encoding JW LHB is slightly longer than the LHB mRNAs of the other two breeds. The NZW and Dutch rabbit LHB coding sequences are 426 bp long, and their G + C contents are higher (>73%) than those of other mammalian LHBs (<70%). The predicted 141-amino-acid sequences of the JW and NZW LHB proteins are identical, and the Dutch LHB and JW/NZW sequences differ at only two residues. The exon–intron configuration of the NZW LHB gene (three exons and two introns) is similar to that of other mammalian LHB genes, and the sequences of NZW rabbit and other mammalian LHB promoter regions are highly conserved. Phylogenetic analysis of the deduced amino acid sequences of the three rabbit LHB proteins indicated that the rabbit occupies a phylogenetic position between rodents and domestic animals, and is far from humans. The results suggest that LH prepared from rodents or domestic animals, if available, would be a better inducer for superovulation in rabbits than human LH/CG.

Keywords: LHB; Phylogeny; Breed; Promoters

1. Introduction

Gonadotropin treatment is routinely used to induce superovulation in laboratory animals. To examine the molecular basis of this induction, we previously determined and compared the cDNA sequences of the pituitary gonadotropin subunits and their receptors in several animals (Suzuki et al., 2002, 2003; Koura et al., 2004; Takano et al., 2004; Noguchi et al., 2006). Combined with the sequences of other animals (reviewed by Bousfield et al., 1994), we found that homology between exogenous and endogenous gonadotropins is a key factor in efficient induction of superovulation. In the present study, we determined and characterized the cDNA, and predicted amino acid sequences of the luteinizing hormone β-subunit (LHB) precursor protein in three breeds of rabbit, and we performed a phylogenetic analysis of these LHB protein sequences and those of other mammalian species. In addition, the genomic sequence of the LZW rabbit LH gene was determined using PCR analysis of introns and genomic walking. We discuss the possibility of using sequence information as a criterion for selecting gonadotropins for rabbit superovulation.

2. Materials and methods

2.1. Determination of rabbit LHB cDNA sequences

We determined the complete sequences of LHB cDNAs from three breeds of rabbits using 5′- and 3′-rapid amplification of cDNA ends

* Corresponding author. Fax: +81 72 641 9857.
E-mail address: osuzuki@nibio.go.jp (O. Suzuki).

0016-6480/$ - see front matter © 2006 Elsevier Inc. All rights reserved.
doi:10.1016/j.ygcen.2006.09.012

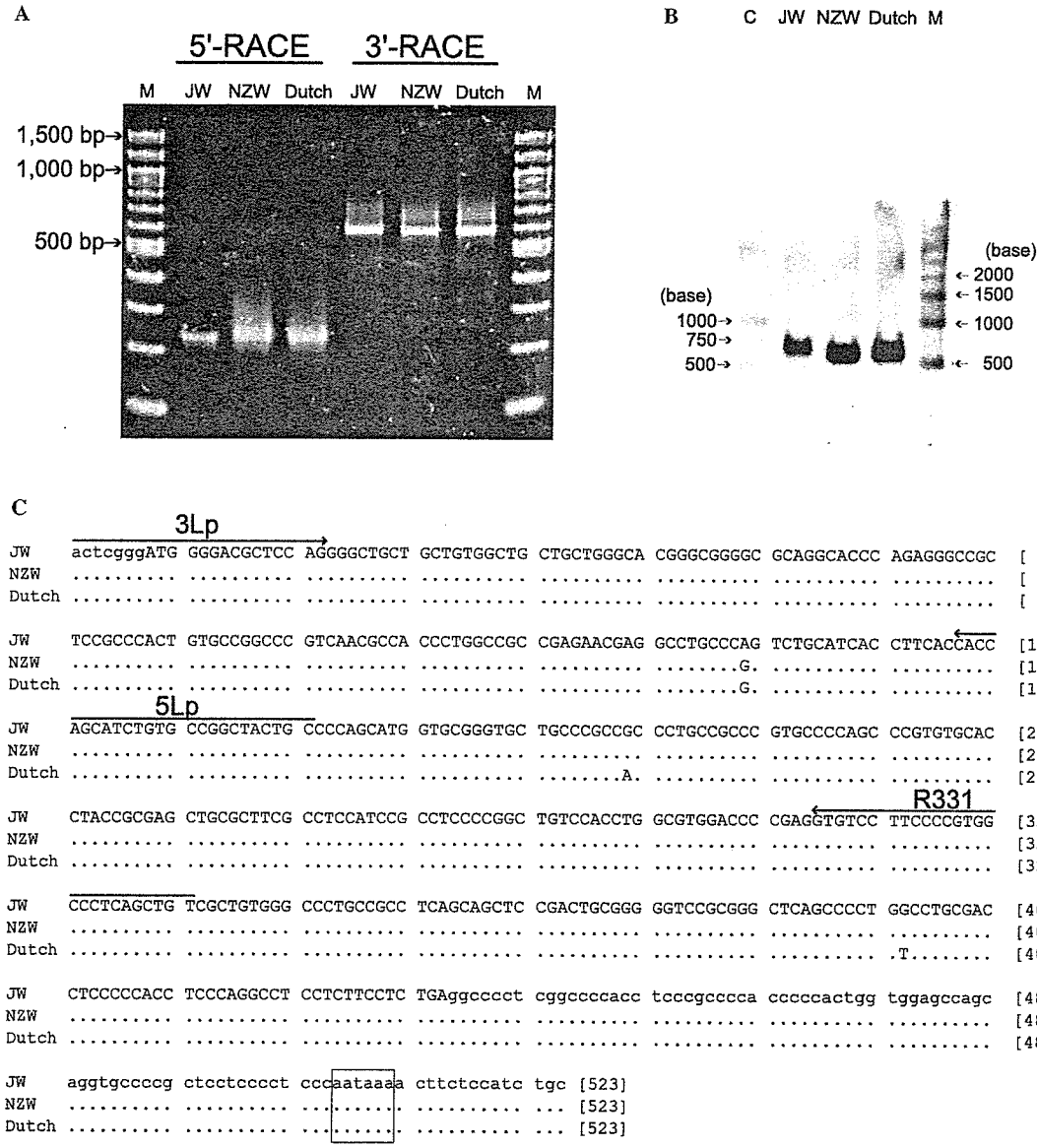

Fig. 1. (A) The products of 5′- and 3′-rapid amplification of cDNA ends (RACE) of LHB genes from JW, NZW, and Dutch rabbits were resolved on 2% agarose gels. M: 100-bp ladder. (B) Northern blot hybridization analysis of rabbit LHB mRNAs. C: RNA Century Markers; M: BrightStar Biotinylated RNA Millennium Markers (Ambion). (C) Alignment of LHB cDNAs from JW and NZW rabbits. Lowercase letters indicate the 5′- and 3′-untranslated regions, and uppercase letters indicate the coding sequence. Putative polyadenylation signal sequences are boxed. Arrows indicate the positions of primers 5Lp and 3Lp. A dot indicates a nucleotide that is identical at the corresponding site in the JW sequence (top row).

(RACE) followed by direct sequencing of the RACE products, as described previously (Noguchi et al., 2006). RACE was performed using the SMART™ RACE cDNA Amplification Kit (Clontech Laboratories, Mountain View, CA) with cDNA libraries prepared from pituitary total RNA samples (~1 μg). Japanese White rabbit (JW) pituitary tissues were purchased from Funakoshi (Tokyo, Japan), and New Zealand White (NZW) and Dutch-Belted (Dutch) rabbit pituitary tissues were from Kitayama Labes (Ina, Japan). RACE reactions were performed with Hot-StarTaq DNA polymerase and Q-Solution (both from Qiagen, Hilden, Germany) with initial denaturation and enzyme activation at 94 °C for 15 min, followed by 40 cycles of 94 °C for 2 s and 68 °C for 5 min.

The positions of the gene-specific primers used in the RACE reactions are shown in Fig. 1C. Initially, 5′-RACE was conducted with the gene-specific primer 5Lp (5′-ACAGTAGCCGGCACAGATGCTGGTGGT-3′), which was designed from the mastomys LHB sequence (AY353073 from GenBank, Takano et al., 2004). The sequence of the 5′-RACE product from JW rabbit was used to design the gene-specific primer 3Lp (5′-ACTCGGGATGGG GACGCTCCAG-3′). The 3′-RACE reactions were performed with 3Lp, and the sequence of the 3′-RACE product was determined. Both primers were used to sequence the LHB cDNAs of the NZW and Dutch rabbits. All of the RACE products were gel-purified and sequenced as previously described (Noguchi et al., 2006), and full-length sequences were obtained by combining the overlapping sequences of the 5′- and 3′-RACE products.

2.2. Northern blot analysis

Northern blot analysis was performed using the NorthernMax-Gly Kit (Ambion, Austin, TX) with 3 μg of pituitary total RNA from each breed and biotinylated RNA size-markers. Biotinylated DNA probes (331 bp) were generated by PCR using the JW cDNA with primers 3Lp and R331

(5′-ACAGCTGAGGGCCACGGGGAAGGACAC-3′; see Fig. 1C for primer positions) and labeled using the *Label*IT Biotinylation Kit (Mirus Bio, Madison, WI). After overnight hybridization at 42 °C, the hybridization signals and size-markers were detected by chemiluminescence using the BrightStar BioDetect Kit (Ambion). Images were captured using a CCD camera (LAS-3000, Fuji Photo Film Co. Ltd., Tokyo, Japan).

2.3. Molecular phylogenetic analysis

The following mammalian LHB cDNA sequences were retrieved from GenBank (Accession Nos. in parentheses): mouse (NM_008497), rat (NM_012858), pig (NM_214080), cattle (NM_173930), sheep (NM_001009380), human (NM_000894), Mongolian gerbil (AY369077), mastomys (AY353073), Guinea pig (AY373317), Syrian hamster (AY353074), cat (NM_001009277), and crab-eating macaque (AJ781396). The amino acid sequences predicted by these cDNAs and the three rabbit LHB cDNAs were aligned using CLUSTAL W software (Thompson et al., 1994). A neighbor-joining tree containing the LHB protein sequences of 15 animals was constructed using MEGA3.1 software (Kumar et al., 2004) based on the Jones-Taylor-Thornton matrix model (Jones et al., 1992) with 5000 bootstrap iterations.

2.4. Determination of the LHB genomic DNA sequence

The genomic sequence of NZW rabbit LHB was determined (Seegene, Inc., Seoul, Korea) by analysis of the introns and flanking sequences. To sequence the introns, the following sets of primers were applied directly to the genomic PCR: 3Lp and R511 (5′-GTTTTATTGGGAGGGGAGGA GCGGGGC-3′); 3Lp and R331 (5′-ACAGCTGAGGGCCACGGGGA AGGACAC-3′), and 3Lp and 5Lp. The positions of these primer sites are shown in Fig. 3. The genome walking technique was used to determine the upstream (5′-flanking) and downstream (3′-flanking) sequences of the LHB gene using the GenomeWalker Universal Kit (Clontech). Adaptor-ligated genomic DNA libraries were constructed according to the kit protocol. Primary PCR amplifications were performed using an initial denaturation temperature of 94 °C (15 min) followed by 40 cycles of 94 °C (2 s) and 68 °C (5 min). Nested PCR was performed similarly except that 30 cycles were employed instead of 40 cycles. The sequences of the PCR products were determined by the method used in the RACE experiments, and the genomic sequence encompassing the exons, introns, and flanking sequences was constructed by combining the PCR-generated overlapping sequences. The numbers and locations of the exons were determined by comparisons with the cDNA sequence. The following primers were used (see Fig. 3 for primer positions): upstream primary, R1099 (5′-CAC CATGCTGGGGCAGTAGC-3′); upstream nested, 5Lp; downstream primary, S1285 (5′-GTGCCCCAGCCCGTGTGCACCTACC-3′); and downstream nested, S1471 (5′-CACCTCCCAGGCCTCCTCTTCCTCT GA-3′).

Additional LHB genomic sequences for mice (NC_000073), rats (J00749), cattle (M11506), and humans (NC_000019) were retrieved from GenBank. The exon–intron configurations of the LHB genes in these mammals plus rabbits are illustrated in Fig. 3B. In Fig. 3C, we compare the binding sites for various transcription factors in the 5′-flanking sequences of the LHB genes, which were aligned using CLUSTALW.

3. Results and discussion

The RACE experiments identified LHB transcripts in the pituitary cDNA libraries of all three rabbit breeds (Fig. 1A). These full-length LHB sequences are shown in Fig. 1C. All of the cDNA sequences were 523 bp in length (from the 5′-terminus to the putative polyadenylation site, with a short 5′-untranslated region of 7 bp). The RACE experiments indicated the presence of only a single LHB mRNA species in the pituitary library, and Northern blot analyses confirmed the presence of single LHB transcripts (Fig. 1B). The transcripts isolated from the JW rabbits were slightly longer than those isolated from the NZW and Dutch rabbits, possibly due to length polymorphism of the polyA tail. The sequences have been deposited in the DDBJ/EMBL/GenBank databases under Accession Nos. AB235913, AY614703, and AB235914 for the NZW, JW, and Dutch rabbit breeds, respectively.

The rabbit LHB coding sequences have higher G + C contents (>73%) than those of other mammals (63–70%). Among the LHB cDNA sequences, we found that the JW and NZW sequences differ at one nucleotide (nt); the NZW and Dutch sequences differ at two nts; and the JW and Dutch sequences differ at three nts. These nt sequence differences do not cause the predicted NZW and JW amino acid sequences to differ, but they do cause the Dutch amino acid sequence to differ from the NZW/JW sequence at two positions. This difference reflects the distant relationship between the Dutch breed and the JW and NZW breeds. The similarity noted between the JW and NZW breeds may reflect the fact that an NZW × JW cross was made during establishment of the JW breed.

Alignments of the predicted amino acid sequences of the rabbit LHBs and other mammalian LHBs reveal that the rabbit sequences are 73–90% similar to the other LHBs (Fig. 2A), and that the positions of the cysteine residues and putative N-glycosylation sites are highly conserved. Although the 19th amino acid residue of the rabbit LHB precursor protein corresponds to the first residue of the mature protein (Glenn et al., 1984), most LHB precursor proteins contain signal sequences of 20 residues. Thus, in determining the homology matrix for the signal (upper-right triangle) and mature (lower-left triangle) LHB sequences from 15 different animal species (Fig. 2B), we made the assumption that the 23rd amino acid residue in Fig. 2A corresponds to the first residue of the mature protein. The signal sequences of the rabbit LHB precursor proteins are moderately conserved (59–77%), whereas the mature protein sequences are highly conserved (73–93%).

For each of the three rabbit breeds used in this study, our results indicate that the putative N-terminus of the mature LHB corresponds to QAPRG; this result differs from the QPARG motif reported as the N-terminal sequence of mature LHB (Glenn et al., 1984). This discrepancy may be a result of differences among the breeding colonies used to obtain pituitary samples. However, if the mature protein with an N-terminal QPARG motif is indeed produced from the cDNA encoding the QAPRG motif, then the LHB processing mechanism in the rabbit merits further investigation. Our cDNA sequencing results confirm that C-terminal processing occurs during formation of mature LHB; the predicted C-terminal amino acids are LLFL, but these residues were not detected by protein sequencing (Glenn et al., 1984). Thus, our results agree with the suggestion by Glenn et al. (1984) that both ends of the rabbit LHB precursor protein are removed during the maturation process.